Methodology for Imaging Nano-to-Microscale Water Condensation Dynamics on Complex Nanostructures

Konrad Rykaczewski* and John Henry J. Scott

Material Measurement Laboratory, National Institute of Standards and Technology, Gaithersburg, Maryland 20899-8320, United States

ABSTRACT A better understanding of the role that nanoscale surface chemical heterogeneities and topographical features play in water droplet formation is necessary to improve design and robustness of nanostructured superhydrophobic surfaces as to make them fit for industrial applications. Lack of an imaging method capable of capturing the water condensation process on complex nanostructures with required magnification has thus far hindered experimental progress in this area. In this work, we demonstrate that by transferring a small part of a macroscale sample to a novel thermally insulated sample platform we are able to mitigate flooding and electron heating problems typically associated with environmental scanning electron microscopy of water condensation. We image condensation dynamics on individual complex particles and a superhydrophobic network of nanostructures fabricated from low thermal conductivity materials with an unobstructed 90° perspective of the surface-to-water interface with field of view as small as 1 μm^2. We clearly observe the three-stage drop growth process and demonstrate that even during late stages of the droplet growth the nearly spherical drop remains in a partially wetting Wenzel state.

KEYWORDS: complex nanostructures · environmental scanning electron microscopy · superhydrophobicity · nanoscale water condensation · focus ion beam · wet-STEM

Our understanding of the role that surface chemical heterogeneities[1−4] and topographical features[5−10] play in water droplet formation is just beginning to emerge. The nanoscale feature size of superhydrophobic surfaces (SHS) makes studying of such effects particularly challenging. While most SHS can be wet completely following sufficient condensation, when droplets form on selected natural[2,11,12] and artificial[5,6,13−16] surfaces, they adopt nearly spherical shapes and become highly mobile.[5,13,14] A better understanding of how droplets form on the SHS which retain their superhydrophobic characteristics during condensation would aid in the design and industrial application of SHS as promoters of the highly efficient dropwise condensation process.[5] In order to study the influences of the local topography and the spatial heterogeneity of surface properties on droplet condensation, an imaging technique with nanoscale spatial resolution and fast temporal resolution is necessary. Atomic force microscopy (AFM) and environmental scanning electron microscopy (ESEM) are two methods capable of imaging water droplets with the required spatial resolution.[17] AFM is not capable of imaging three-dimensional topological features such as randomly stacked nanowires[5,18] or ribbed nanoneedles[19] and is too slow to capture the fast dynamics of the condensation process. A number of issues also arise during ESEM imaging of the nano-to-microscale condensation dynamics on macroscale samples with nanoscale topographical features. First, the macroscale size of the sample prevents imaging at high viewing angles. Second, even when very small samples are employed, part of the sample is obstructed by the local microscale topography such as neighboring nanowires or nascent water droplets.[20] Third, secondary electrons originating in the bulk substrate can significantly contribute to the total secondary electron (SE) signal when imaging drops less than 1 μm in diameter,[21] complicating image interpretation. Lastly, electron beam heating can cause rapid evaporation of condensed drops and thus limits the range of useful imaging magnifications.[10] Because the electron beam heating effects are more pronounced on substrates with low thermal conductivity,[10] imaging of condensation on SHS made out of natural,[2,11,22,23] polymer,[24,25] and oxide[5,18,19,26] materials is particularly difficult. In this work, we introduce a new approach for *in situ* ESEM condensation imaging that avoids the substrate-related imaging issues by removal and transfer of a small part of the macroscale substrate to a thermally insulated sample platform. Specifically, micromanipulation and focused ion beam (FIB)

* Address correspondence to konrad.rykaczewski@nist.gov.

Received for review May 11, 2011 and accepted June 10, 2011.

Published online June 11, 2011
10.1021/nn201738n

micromaching are used to transfer a small section of the original sample to an exposed portion of a thin metal grid partially encapsulated in a thick thermal insulator. The small size and perpendicular orientation of the sample with respect to the electron beam limit the absorbed energy and enable simultaneous visualization using secondary and transmitted electrons. The thermally insulating coating over the high thermal conductivity metal grid encourages water condensation preferentially on the exposed metal area and the attached sample. To compare this new approach to current strategies of sample preparation for ESEM imaging, we image water condensation on thermally insulating nanowhisker-decorated copper oxide (CuO) particles drop-casted onto a metal block,[27−29] a carbon foil,[30−33] and attached to the thermally insulated sample platform. We demonstrate that our approach allows for high-magnification imaging while mitigating heating and flooding problems often encountered when using standard imaging strategies. To further demonstrate the enhanced capabilities of this new methodology, we image condensation on a small section of a low thermal conductivity superhydrophobic $Cu(OH)_2$ nanowire network,[5,18,34] a task that has proven to be very challenging in the past. With a wide, 90° unobstructed perspective, we clearly observe the three-stage drop growth process previously observed solely from a top-down view[10] and demonstrate that, even during late stages of the droplet growth, the nearly spherical drop remains in a partially wetting Wenzel state.

RESULTS AND DISCUSSION

Fabrication of the imaging platform and the microscale sample preparation are achieved using a combination of simple coating, micromanipulation, and FIB micromaching steps. To fabricate the thermally insulated sample platform, a commercially available copper (Cu) TEM half-grid with several extended posts is partially dipped in a small drop of liquid cyanoacrylate adhesive and allowed to dry. This coats the Cu grid with a solid exhibiting low thermal conductivity[35] (≈0.5 W/mK); the resulting coating thickness is between 100 and 200 μm (see Figure 1a). To avoid charging problems, a 50 nm gold layer is sputtered on both sides of the coated grid to improve electrical conductivity. The cyanoacrylate coating is milled away locally using the FIB to expose a metallic Cu area approximately 5 μm × 10 μm in lateral extent. Figure 1a shows that the Cu area is surrounded by cyanoacrylate and orientated at 90° with respect to the rest of the metal grid surface and, when mounted in the ESEM, the electron beam. Next, a section of the original macroscale sample is transferred to the exposed Cu area. An example of the whole process is illustrated in Figure 1b, which shows the transfer of a CuO particle. After being attached to a

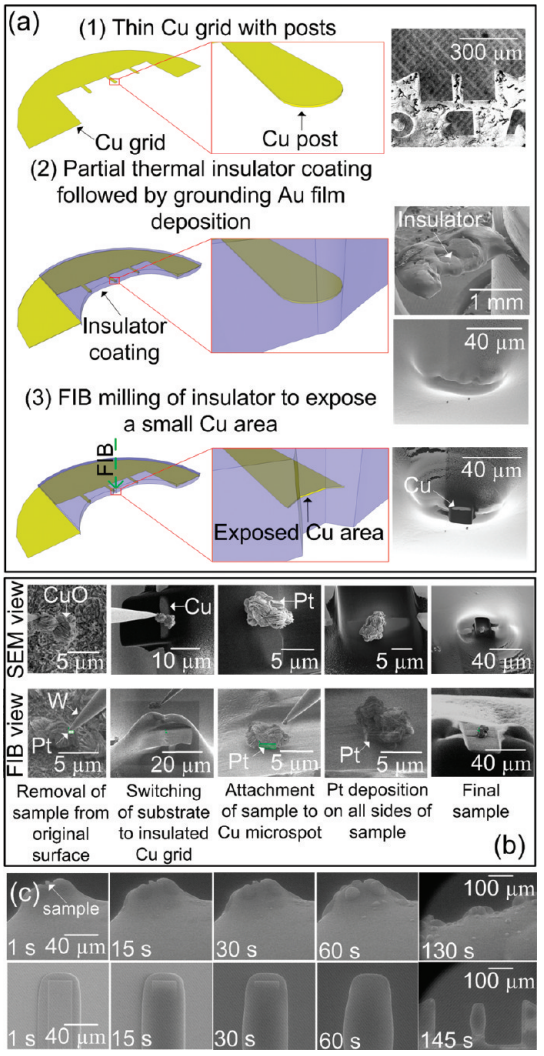

Figure 1. (a) Schematic and SEM images of the fabrication process of the thermally insulated sample platform. (b) SEM and FIB images showing the transfer of a CuO microparticle from the original substrate to the exposed Cu area on the sample platform (the viewing perspective of the FIB images is oriented at 52° with respect to the SEM images). (c) Comparison between condensation dynamics on a coated (top) and an uncoated Cu grid (bottom) mounted in the cooling stage with a temperature decrease from 3 to 0 °C with background water vapor pressure of 650 Pa.

tungsten needle with a platinum (Pt) pad created by focused ion beam induced deposition, the CuO particle is lifted from the original surface and lowered onto the exposed Cu area. If the desired part of the sample is firmly attached to the original surface, a wedge-like section of the surface is cut away using the focused gallium ion beam prior to attachment of the needle.[36] After the CuO particle is attached to the Cu area using a Pt pad, the Pt pad connecting the particle and the needle is milled away using the ion beam. In the final step, a Pt pad is deposited around the whole Cu surface and particle interface by three iterations of 90° sample rotation and Pt pad deposition steps. The deposited "Pt" material contains about 80% low thermal conductivity amorphous carbon.[37] We found that a 500 nm Pt

pad thickness helps to reduce the thermal contact resistance of the particle and surface interface while avoiding significant secondary Pt deposition on the sample.

The partial cyanoacrylate coating on the Cu grid allows for initiation of condensation on the exposed Cu area prior to condensation on the thermal insulator surface. Figure 1c shows that condensation first occurs on the exposed Cu area with a stepwise decrease in the cooling stage temperature from 3 to 0 °C with background water vapor pressure of 650 Pa. During the next 30−60 s, condensation slowly propagates outward on the thermal insulator surface. For comparison, Figure 1c also shows that a whole uncoated Cu post is wetted within 15 s of initiation of condensation (see movie 1 in Supporting Information). As we will demonstrate next, the time delay in water flooding of the sample area gained through the thermal insulation of the Cu grid is sufficient for capturing the nano-to-microscale condensation dynamics on the CuO particles.

To demonstrate the advantages of the new method, we image condensation on CuO particles drop-casted onto a metal block, a carbon foil, and attached to the thermally insulated sample platform. Schematics of the three arrangements and the corresponding thermal resistance networks are shown in Figure 2. In all cases, water condensation is initiated by reducing the temperature of the cooling stage from 3 to 0 °C with a background water vapor pressure of 650 Pa. On the steel block, the temperature decrease quickly inducing water condensation on and around the CuO particles. Figure 3a shows that the quick flooding of the block surface causes physical movement of the CuO particle. As indicated by white arrows in the SEM image series in Figure 3a, the CuO particle rotates over 180° with respect to its original position within 13 s of the beginning of water condensation (see movie 2 in Supporting Information). The particle movement, which does not occur when condensing water on thermally conductive particles such as carbon nanopipes deposited on a steel block,[27,29] can be alleviated by attaching the CuO particle to the substrate using a Pt pad. The fast surface flooding, in turn, is avoided when cooling the carbon foil on a Cu supportive mesh (Figure 3b,c). Condensation occurs much slower on the foil than on the surface of the steel block, most likely due to the high thermal resistance of the carbon foil. However, once condensed on the carbon foil, the water droplets are susceptible to electron beam heating effects even at low imaging magnification[33] (see movies 3 and 4 in Supporting Information). The SEM image series in Figure 3b,c clearly shows fast evaporation of water drops condensed directly on the carbon foil and on the CuO particles on top of the carbon foil. The rate of evaporation increases with increasing magnification[10] and increasing drop size because of corresponding

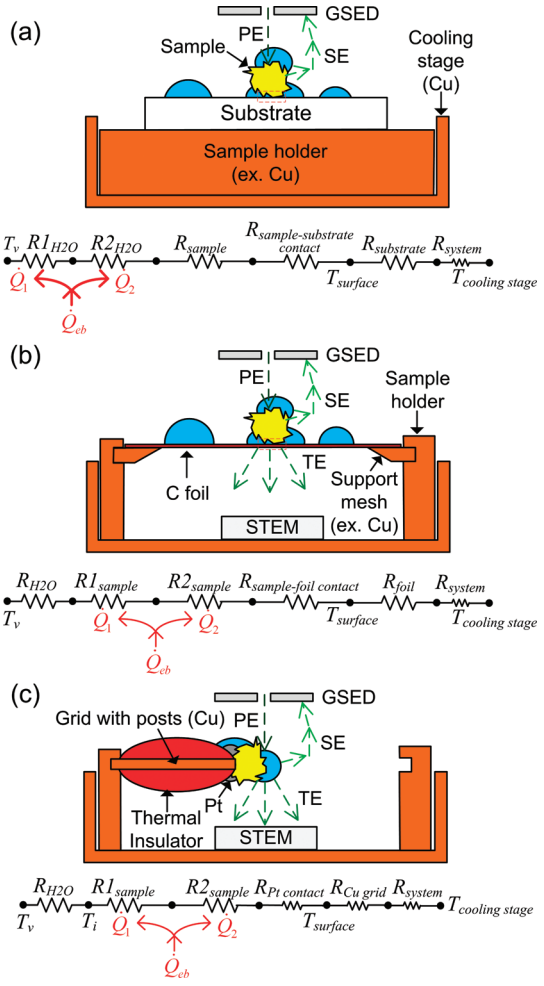

Figure 2. Schematic representation and thermal resistance networks corresponding to the process of imaging of water condensation on CuO particles (a) drop-casted onto a steel block, (b) drop-casted onto a carbon foil on Cu supportive mesh, and (c) attached to the thermally insulated sample platform. PE, SE, and TE stand for primary, secondary, and transmitted electrons while $\dot{Q}_{eb}$, $\dot{Q}_1$, and $\dot{Q}_2$ are for the total absorbed power and its portions conducted away through the liquid−vapor interface and the sample.

increase in the electron flux and the absorbed electron energy. The rate of evaporation also increases if the drop is condensed on the particle because of increased absorbed electron energy within the particle itself and because of additional thermal resistance of the particle and carbon foil to particle interface.

The quick flooding and the strong electron beam heating effects are mitigated during imaging of condensation on the CuO particle attached to the thermally insulated sample platform. As a result, we are able to image wetting and filling of 100−500 nm gaps between 75 and 250 nm nanowhiskers, leading to the formation of a 400−500 nm drop with a viewing field as small as 1 μm × 1 μm. Although the increase in the drop growth time (30 *vs* 15 s) that we observed when changing field of view from 2 μm × 2 to 1 μm × 1 μm

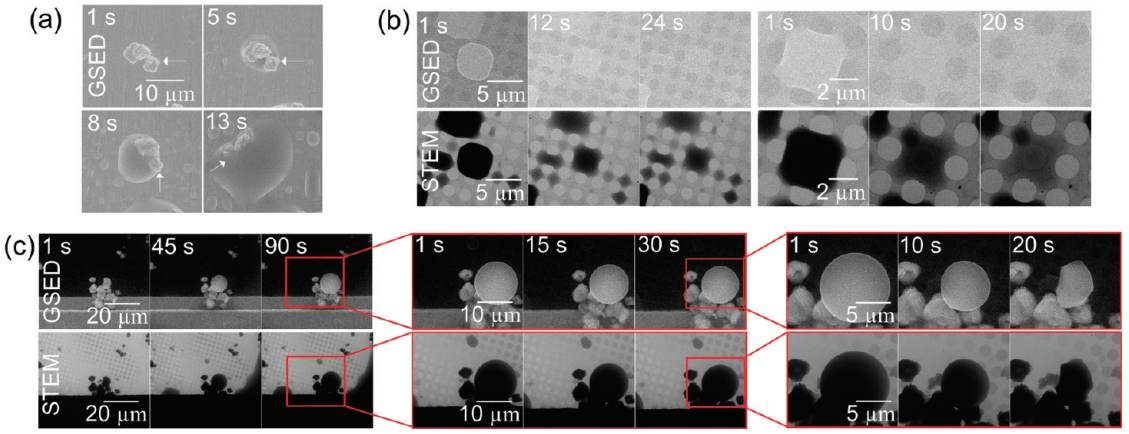

Figure 3. Series of SEM images illustrating (a) flooding and particle displacement and (b,c) electron beam heating problems during imaging of water condensation on CuO particles (a) drop-casted onto a steel block and (b,c) drop-casted onto a carbon foil on Cu supportive mesh. In all cases, water condensation is achieved by the reduction of the cooling stage temperature from 3 to 0 °C with a background water vapor pressure of 650 Pa.

indicates that some electron beam heating effects are still present, this situation is clearly much improved since attempting to image condensation on the original CuO surface using similar magnifications typically causes the drop to evaporate completely within a few seconds.[10] Because comparable magnification condensation imaging has so far only been achieved for highly conductive nanostructure and substrate pair,[27,29] the high-magnification imaging of condensation on the insulating CuO particle is likely to be enabled by the improved heat transfer away from the sample in our setup. Lastly, performing the same experiment at a large viewing field of 10 μm × 10 μm demonstrates the advantages of viewing the drop formation with an unobstructed 90° perspective. The surface-to-water interface is clearly visible throughout the entire drop formation process in Figure 4 (see movie 5 in Supporting Information).

The ability to image the surface-to-water interface is crucial in developing an understanding of the wetting behavior of water on SHS. Accordingly, we apply the methodology developed in this work to image condensation on a section of superhydrophobic $Cu(OH)_2$ nanowires, which do retain their superhydrophobic properties during condensation.[5,10,18] During the sample fabrication process, care must be taken to minimize the sample modification from ion beam exposure and unintentional material redeposition from sputtering. The SEM images in Figure 5 demonstrate that the FIB prepared section of the $Cu(OH)_2$ nanowire network retains the superhydrophobic characteristics of the original surface (see Methods section for fabrication details). The nanowire network section has a significantly higher thermal resistance than the CuO microparticle sample. Consequently, it is difficult to preferentially induce condensation on the attached nanowires solely by varying the temperature of the cooling stage, and the commonly used technique of varying the pressure is required to achieve the desired result.[1−3,7,17,20,27,30−33] In this technique, water condensation is induced by a pressure increase from 600 to 650 Pa while holding the temperature of the holder and platform constant at 0 °C. Individual drop condensation during this procedure proceeds according to the previously proposed three-stage growth mechanism.[10] First, previously nucleated drops less than 1 μm in diameter coalesce, causing the condensation to wet and fill an area between the nanowires (drops are highlighted by white arrows in the top SEM image sequence in Figure 5). The characteristic dimension of this area is approximately 2−4 μm across. Subsequently, a liquid drop begins to emerge from the wetted area. This drop emergence is driven by an increase in the contact angle between the drop and a base area of constant size. The drop reaches a near spherical shape and switches from a near-constant-base area growth mode to a near-constant-contact angle mode when it reaches a diameter of approximately 4−6 μm. On the macroscale sample, the droplet continues to grow until it coalesces with neighboring drops, flooding the surrounding portion of the sample. Using the new approach, the drop collapses when it comes in contact with the edge of the Cu grid about 15 μm away from where it originated. The high-magnification SEM images in the bottom of Figure 5 show that even minutes into the growth process the nearly spherical drop remains in a partially wetting Wenzel state, despite having grown to a diameter of 10−20 μm (see movie 6 in Supporting Information). Since we previously observed high droplet mobility and departure of 300 μm condensed water drops from the macroscale sample of SHS formed from randomly stacked $Cu(OH)_2$ nanowires,[10] this result implies that a larger drop diameter is necessary for the theoretically predicted[38,39] Wenzel to Cassie state transition to occur on this surface.

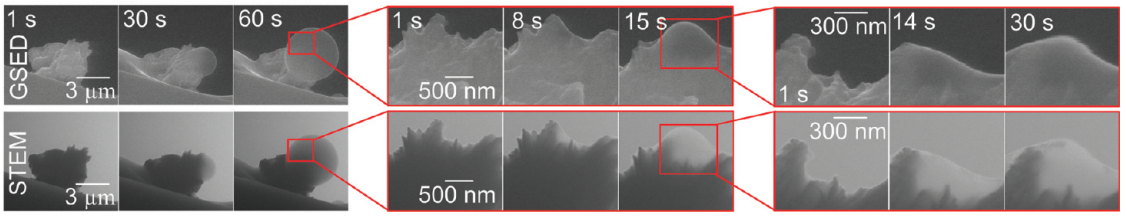

Figure 4. Series of SEM images illustrating micro- and nanoscale imaging of water condensation on CuO particles attached to the thermally insulated sample platform. In all cases, water condensation is achieved by the reduction of the cooling stage temperature from 3 to 0 °C with a background water vapor pressure of 650 Pa.

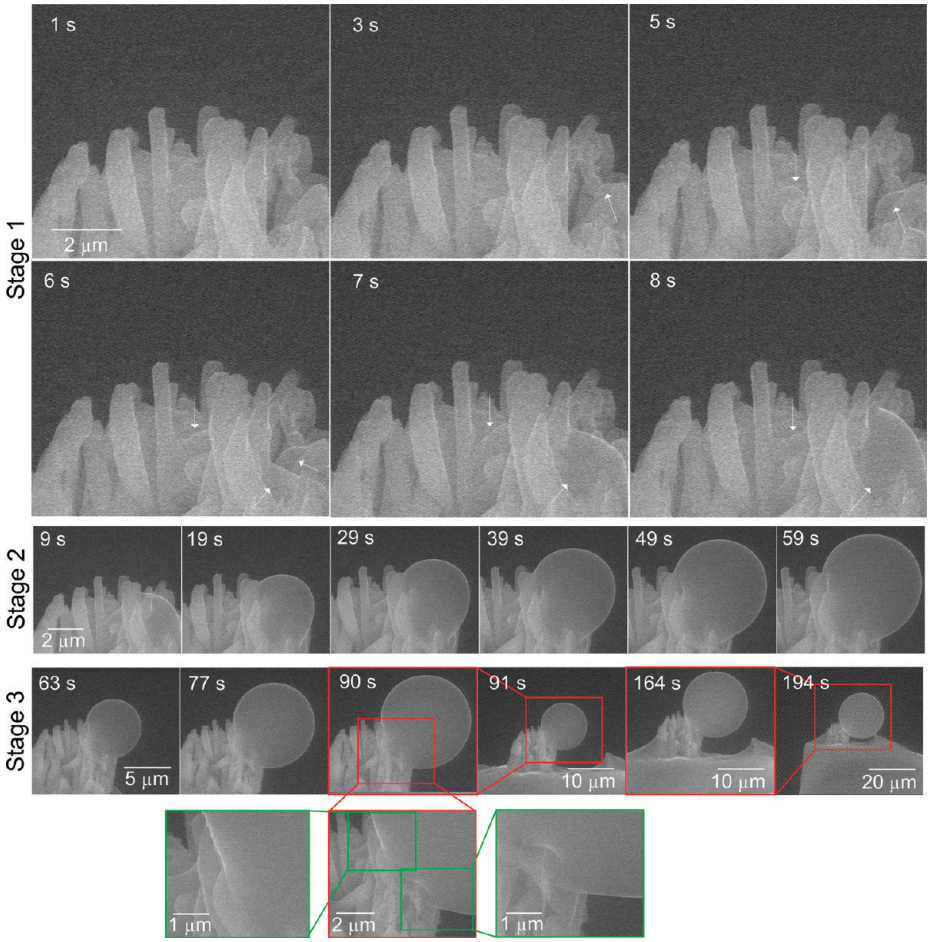

Figure 5. SEM image series of the three-stage water droplet growth process on a section of SHS formed from randomly stacked $Cu(OH)_2$ nanowires.

In conclusion, we introduce a new approach for *in situ* ESEM imaging of nano-to-microscale condensation dynamics on complex nanostructures. The approach consists of transferring a small part of a macroscale sample to a novel thermally insulated sample platform on which preferential condensation can be achieved. We demonstrated that imaging of condensation on the CuO particle attached to the thermally insulated sample platform is advantageous because it mitigates the quick sample flooding and the strong electron beam heating problems associated with current imaging strategies of low thermal conductivity samples. As a result, we imaged wetting and filling of gaps between nanowhiskers leading to the formation of a 400−500 nm water drop; this was accomplished with an imaging field of view as small as 1 μm × 1 μm. Furthermore, the unobstructed 90° perspective allowed us to image the interface between the surface under study and the water during the entire drop formation process. Using the new approach, we obtained images of water condensation on a section of a superhydrophobic $Cu(OH)_2$ nanowire network that support the three-stage drop growth mechanism. We were also able to determine that even nearly spherical drops with diameters as large as 20 μm remain in a partially wetting

Wenzel state. The methodology introduced in this work should be appropriate for high-magnification imaging of other problems involving water phase changes, such as water evaporation from nanopores[40,41] and ice formation on icephobic nanostructures.[42−44]

METHODS

Platform and Sample Fabrication Procedure. The fabrication of the platform and the sample preparation were achieved by a combination of simple coating, micromanipulation, and FIB micromaching steps. All FIB milling and Pt deposition as well as sample micromanipulation were performed using an FEI Nova 600 DualBeam equipped with an Autoprobe 200 nanomanipulation system. All FIB operations were performed with ion beam energy of 30 keV, but the ion current was varied for different steps. For milling the cyanoacrylate coating, milling the $Cu(OH)_2$ nanowire network, Pt pad deposition, and imaging during micromanipulation ion beam currents of 21 nA, 2.8 nA, 0.28 nA, and 9.7 pA were used, respectively. The 200−500 nm thick Pt pads were fabricated using focused ion beam induced deposition (FIBID) from a $C_9H_{16}Pt$ gas precursor using a dwell time of 200 ns per pixel. During fabrication, all structures were imaged at 0 or 52° tilt using an electron beam current of 98 pA and electron beam energy of 5 keV.

To fabricate the platform, Omniprobe Cu lift-out grids with three posts were coated with a small drop of liquid cyanoacrylate (Krazy Glue) and allowed to dry in an ambient room environment for 2−3 h. The coating procedure resulted in a solid cyanoacrylate coating with a thickness of 100−200 μm. To minimize electrical charging, a 50 nm gold layer was sputtered on both sides of the coated grid using a Cressington 208 HR sputter coater equipped with a quartz microbalance thickness monitor. Next, the cyanoacrylate coating was locally milled away using the ion beam until a tip of a Cu post is exposed. Because of the perpendicular grid and ion beam column orientation, the exposed Cu area was orientated at 90° with respect to the rest of the metal grid surface.

The procedure for transferring a CuO microparticle from the original sample is outlined in the paper. To remove a section of the $Cu(OH)_2$ nanowire network, an angled line "U"-shaped cut with dimensions of 5−10 μm was performed at 0° sample tilt. A vertical line cut performed at a sample tilt of 52° completed the release of the cut-out wedge. To facilitate the needle attachment step, a temporary 1 μm × 1 μm wide and 1 μm thick Pt pad was deposited in one corner of the wedge prior to its release. The wedge was attached to the Cu area with an orientation correction to maximize the Cu to wedge contact area. The volume containing the temporary Pt pad was milled away after the wedge attachment and needle release.

ESEM Imaging Procedure. The condensation experiments were performed in a FEI Quanta 200 FEG ESEM whose stage temperature was controlled with a water-cooled thermoelectric (Peltier effect) element. The water vapor pressure in the ESEM chamber was controlled using the microscope's differential pumping system and gas delivery manifolds. The Cu grids were attached to the Cu TEM grid holder for the cooling stage. Water condensation was achieved by either varying the cooling stage temperature or by varying of the chamber pressure with specific conditions corresponding to different experiments indentified in the paper. Besides the fabricated sample platform, carbon Quantifoil TEM Cu mesh with an orthogonal array of 1.2 μm diameter holes was used, as well as a 1 cm diameter steel block substrate. The samples were simultaneously imaged using the gaseous secondary electron detector (GSED) and the scanning transmission electron microscopy detector (STEM) with a frame time of 1 s. Images were captured with a 1 Hz frequency. To minimize the absorbed energy, condensation was imaged at a low electron beam current (0.08 nA) in all arrangements. Different electron beam energies were used to minimize the absorbed energy for bulk and thin samples. For the CuO particle drop-casted onto a steel block, the lowest possible electron beam energy providing acceptable image quality for a given working distance and background pressure was used (10 keV).[10] In contrast, condensation on CuO drop-casted onto the carbon foil or attached to the thermally insulated sample platform was imaged with electron beam energy of 30 keV because electron energy loss (and therefore energy deposition in the sample) decreased with increasing electron energy.[45]

Acknowledgment. This research was performed while K.R. held a National Research Council American Recovery and Reinvestment Act (NRC ARRA) Research Associateship at the National Institute of Standards and Technology in Gaithersburg, MD. The authors acknowledge C. Dietz and Y.K. Joshi from Georgia Institute of Technology for providing samples of CuO and $Cu(OH)_2$ surfaces. Certain commercial equipment, instruments, and materials are identified in this publication to adequately specify the experimental procedure. Such identification in no way implies approval, recommendation, or endorsement by NIST, nor does it imply that the equipment, instruments, or materials identified are necessarily the best available for the purpose.

Supporting Information Available: Movies of all condensation experiments performed in the paper. This material is available free of charge *via* the Internet at http://pubs.acs.org.

REFERENCES AND NOTES

1. Varanasi, K. K.; Hsu, M.; Bhate, N.; Yang, W.; Deng, T. Spatial Control in the Heterogeneous Nucleation of Water. *Appl. Phys. Lett.* **2009**, *95*, 094101-1–094101-3.
2. Zheng, Y. M.; Han, D.; Zhai, J.; Jiang, L. *In Situ* Investigation on Dynamic Suspending of Microdroplet on Lotus Leaf and Gradient of Wettable Micro- and Nanostructure from Water Condensation. *Appl. Phys. Lett.* **2008**, *92*, 084106-1–084106-3.
3. Aronov, D.; Rosenman, G.; Barkay, Z. Wettability Study of Modified Silicon Dioxide Surface Using Environmental Scanning Electron Microscopy. *J. Appl. Phys.* **2007**, *101*, 084901-1–084901-5.
4. Daniel, S.; Chaudhury, M. K.; Chen, J. C. Fast Drop Movements Resulting from the Phase Change on a Gradient Surface. *Science* **2001**, *291*, 633–636.
5. Dietz, C.; Rykaczewski, K.; Fedorov, A. G.; Joshi, Y. Visualization of Droplet Departure on a Superhydrophobic Surface and Implications to Heat Transfer Enhancement during Dropwise Condensation. *Appl. Phys. Lett.* **2010**, *97*, 033104-1–033104-3.
6. Lau, K. K. S.; Bico, J.; Teo, K. B. K.; Chhowalla, M.; Amaratunga, G. A. J.; Milne, W. I.; McKinley, G. H.; Gleason, K. K. Superhydrophobic Carbon Nanotube Forests. *Nano Lett.* **2003**, *3*, 1701–1705.
7. Jung, Y. C.; Bhushan, B. Wetting Behaviour during Evaporation and Condensation of Water Microdroplets on Superhydrophobic Patterned Surfaces. *J. Microsc.* **2008**, *229*, 127–140.
8. Nosonovsky, M.; Bhushan, B. Biomimetic Superhydrophobic Surfaces: A Multiscale Approach. *Nano Lett.* **2007**, *7*, 2633–2637.
9. Nosonovsky, M.; Bhushan, B. Patterned Nonadhesive Surfaces: Superhydrophobicity and Wetting Regime Transitions. *Langmuir* **2007**, *24*, 1525–1533.
10. Rykaczewski, K.; Scott, J. H. J.; Fedorov, A. G. Electron Beam Heating Effects During Environmental Scanning Electron Microscopy Imaging of Water Condensation on Superhydrophobic Surfaces. *Appl. Phys. Lett.* **2011**, *98*, 093106-1–093106-3.

11. Mockenhaupt, B.; Ensikat, H.-J. R.; Spaeth, M.; Barthlott, W. Superhydrophobicity of Biological and Technical Surfaces under Moisture Condensation: Stability in Relation to Surface Structure. *Langmuir* **2008**, *24*, 13591–13597.
12. Boreyko, J. B.; Chen, C. H. Restoring Superhydrophobicity of Lotus Leaves with Vibration-Induced Dewetting. *Phys. Rev. Lett.* **2009**, *103*, 174502-1–174502-4.
13. Boreyko, J. B.; Chen, C. H. Self-Propelled Dropwise Condensate on Superhydrophobic Surfaces. *Phys. Rev. Lett.* **2009**, *103*, 184501-1–184501-4.
14. Chen, C. H.; Cai, Q. J.; Tsai, C. L.; Chen, C. L.; Xiong, G. Y.; Yu, Y.; Ren, Z. F. Dropwise Condensation on Superhydrophobic Surfaces with Two-Tier Roughness. *Appl. Phys. Lett.* **2007**, *90*, 173108-1–173108-3.
15. Dorrer, C.; Ruhe, J. Wetting of Silicon Nanograss: From Superhydrophilic to Superhydrophobic Surfaces. *Adv. Mater.* **2008**, *20*, 159–163.
16. Ke, Q.; Zhang, S.; Tang, T.; Wang, S.; Jing, H. Intrinsic Dew-Enhancing Ability of SiO_2/PODS Materials. *Colloids Surf., A* **2011**, *377*, 110–114.
17. Mendez-Vilas, A.; Jodar-Reyes, A. B.; Gonzalez-Martin, M. L. Ultrasmall Liquid Droplets on Solid Surfaces: Production, Imaging, and Relevance for Current Wetting Research. *Small* **2009**, *5*, 1366–1390.
18. Chen, X.; Kong, L.; Dong, D.; Yang, G.; Yu, L.; Chen, J.; Zhang, P. Synthesis and Characterization of Superhydrophobic Functionalized $Cu(OH)_2$ Nanotube Arrays on Copper Foil. *Appl. Surf. Sci.* **2009**, *255*, 4015–4019.
19. Yao, X.; Chen, Q.; Xu, L.; Li, Q.; Song, Y.; Gao, X.; Quéré, D.; Jiang, L. Bioinspired Ribbed Nanoneedles with Robust Superhydrophobicity. *Adv. Funct. Mater.* **2010**, *20*, 656–662.
20. Anand, S.; Son, S. Y. Sub-Micrometer Dropwise Condensation under Superheated and Rarefied Vapor Condition. *Langmuir* **2010**, *26*, 17100–17110.
21. Stelmashenko, N. A.; Craven, J. P.; Donald, A. M.; Terentjev, E. M.; Thiel, B. L. Topographic Contrast of Partially Wetting Water Droplets in Environmental Scanning Electron Microscopy. *J. Microsc.* **2001**, *204*, 172–183.
22. Andrews, H. G.; Eccles, E. A.; Schofield, W. C. E.; Badyal, J. P. S. Three-Dimensional Hierarchical Structures for Fog Harvesting. *Langmuir* **2011**, *27*, 798–3802.
23. Shirtcliffe, N. J.; Brian Pyatt, F.; Newton, M. I.; McHale, G. A Lichen Protected by a Super-hydrophobic and Breathable Structure. *J. Plant Physiol.* **2006**, *163*, 1193–1197.
24. Im, M.; Im, H.; Lee, J.-H.; Yoon, J.-B.; Choi, Y.-K. Analytical Modeling and Thermodynamic Analysis of Robust Superhydrophobic Surfaces with Inverse-Trapezoidal Microstructures. *Langmuir* **2010**, *26*, 17389–17397.
25. Li, X.-M.; Reinhoudt, D.; Crego-Calama, M. What Do We Need for a Superhydrophobic Surface? A Review on the Recent Progress in the Preparation of Superhydrophobic Surfaces. *Chem. Soc. Rev.* **2007**, *36*, 1350–1368.
26. Chinn, J.; Helmrich, F.; Guenther, R.; Wiltse, M.; Hurst, K.; Ashurst, R. W. Durable Super-Hydrophobic Nano-Composite Films. In *NSTI-Nanotech 2010*, 2010; Vol. 1.
27. Rossi, M. P.; Ye, H. H.; Gogotsi, Y.; Babu, S.; Ndungu, P.; Bradley, J. C. Environmental Scanning Electron Microscopy Study of Water in Carbon Nanopipes. *Nano Lett.* **2004**, *4*, 989–993.
28. Rossi, M. P.; Gogotsi, Y.; Kornev, K. G. Deformation of Carbon Nanotubes by Exposure to Water Vapor. *Langmuir* **2009**, *25*, 2804–2810.
29. Mattia, D.; Rossi, M. P.; Kim, B. M.; Korneva, G.; Bau, H. H.; Gogotsi, Y. Effect of Graphitization on the Wettability and Electrical Conductivity of CVD-Carbon Nanotubes and Films. *J. Phys. Chem. B* **2006**, *110*, 9850–9855.
30. Bogner, A.; Thollet, G.; Basset, D.; Jouneau, P. H.; Gauthier, C. Wet STEM: A New Development in Environmental SEM for Imaging Nano-Objects Included in a Liquid Phase. *Ultramicroscopy* **2005**, *104*, 290–301.
31. Bogner, A.; Jouneau, P. H.; Thollet, G.; Basset, D.; Gauthier, C. A History of Scanning Electron Microscopy Developments: Towards "wet-STEM" Imaging. *Micron* **2007**, *38*, 390–401.
32. Barkay, Z. Wettability Study Using Transmitted Electrons in Environmental Scanning Electron Microscope. *Appl. Phys. Lett.* **2010**, *96*, 183109-1–183109-3.
33. Barkay, Z. Dynamic Study of Nanodroplet Nucleation and Growth on Self-Supported Nanothick Liquid Films. *Langmuir* **2010**, *26*, 18581–18584.
34. Zhang, W.; Wen, X.; Yang, S. Controlled Reactions on a Copper Surface: Synthesis and Characterization of Nanostructured Copper Compound Films. *Inorg. Chem.* **2003**, *42*, 5005–5014.
35. Pichardo, J. L.; Alvarado-Gil, J. J. Open Photoacoustic Cell Determination of the Thermal Interface Resistance in Two Layer Systems. *J. Appl. Phys.* **2001**, *89*, 4070–4075.
36. Zaykova-Feldman, L.; Moore, T. M. The Total Release Method for FIB *In-Situ* TEM Sample Preparation. *Microsc. Microanal.* **2005**, *11*, 848–849.
37. Utke, I.; Hoffmann, P.; Melngailis, J. Gas-Assisted Focused Electron Beam and Ion Beam Processing and Fabrication. *J. Vac. Sci. Technol., B* **2008**, *26*, 1197–1276.
38. Liu, T.; Sun, W.; Sun, X.; Ai, H. Thermodynamic Analysis of the Effect of the Hierarchical Architecture of a Superhydrophobic Surface on a Condensed Drop State. *Langmuir* **2010**, *26*, 14835–14841.
39. Koishi, T.; Yasuoka, K.; Fujikawa, S.; Ebisuzaki, T.; Zeng, X. C. Coexistence and Transition between Cassie and Wenzel State on Pillared Hydrophobic Surface. *Proc. Natl. Acad. Sci. U.S.A.* **2009**, *106*, 8435–8440.
40. Narayanan, S.; Fedorov, A. G.; Joshi, Y. K. Gas-Assisted Thin-Film Evaporation from Confined Spaces for Dissipation of High Heat Fluxes. *Nanoscale Microscale Thermophys. Eng.* **2009**, *13*, 30–53.
41. Narayanan, S.; Fedorov, A. G.; Joshi, Y. K. On-Chip Thermal Management of Hotspots Using a Perspiration Nanopatch. *J. Micromech. Microeng.* **2010**, *20*, 075010-1–075010-10.
42. Varanasi, K. K.; Deng, T.; Smith, J. D.; Hsu, M.; Bhate, N. Frost Formation and Ice Adhesion on Superhydrophobic Surfaces. *Appl. Phys. Lett.* **2010**, *97*, 234102-1–234102-3.
43. Meuler, A. J.; McKinley, G. H.; Cohen, R. E. Exploiting Topographical Texture To Impart Icephobicity. *ACS Nano* **2010**, *4*, 7048–7052.
44. Mishchenko, L.; Hatton, B.; Bahadur, V.; Taylor, J. A.; Krupenkin, T.; Aizenberg, J. Design of Ice-Free Nanostructured Surfaces Based on Repulsion of Impacting Water Droplets. *ACS Nano* **2010**, *4*, 7699–7707.
45. Goldstein, J.; Newbury, D. E.; Joy, D. C.; Lyman, C. E.; Echlin, P.; Lifshin, E.; Sawyer, L.; Michael, J. R. *Scanning Electron Microscopy and X-ray Microanalysis*, 3rd ed.; Springer: New York, 2003.